Cathodoluminescence as a method of extracting detailed information from nanophotonics systems: a study of silicon nanocrystals

A. Dowd[a], B. Johansson[a1], N. Armstrong[a], C. Ton-That[a] and M. Phillips[b]

[a]Department of Applied Physics, University of Technology Sydney, NSW 2007, Australia
[b]Microstructural Analysis Unit, University of Technology Sydney, NSW 2007, Australia

ABSTRACT

We investigated Si nanocrystal samples produced by high dose 600 keV Si^+ implantation of fused silica and annealing using cathodoluminescence (CL). CL spectra collected under 5-25 keV electron irradiation show similar features to reported photoluminescence spectra, including the strong near IR peak. The CL intensity distribution is formulated as a linear inverse problem and two methods namely the regularisation method and maximum entropy method can be applied to determine the depth profile without making any assumptions concerning the profile function, i.e. a free form solution. We show using simulated CL data that the maximum entropy method is the most appropriate as it preserves the positivity and additivity of the depth profile. This method is applied to experimental CL data and we have localised the spatial origin of the near IR emission to the near-surface region of the implant, 400 nm from the surface, containing the smallest Si nanocrystals.

Keywords: cathodoluminescence, silicon, nanostructures, maximum entropy, inverse problem

1. INTRODUCTION

Efficient light emission from Si nanocrystals[1] has attracted much interest because of the possible exploitation in Si-based photonics. Si is an indirect gap semiconductor in the bulk form, however quantum confinement results in an increase in band gap and luminescence efficiency in Si nanocrystals. Si nanocrystals can be synthesised in a number of ways including HF etching of Si wafers[2], chemical vapour deposition[3] and ion implantation[4-7]. Implantation is a flexible technique that is fully compatible with today's ULSI technology which introduces excess Si to the near surface region of a variety of host matrices. Post-implantation annealing causes diffusion the Si atoms resulting in spherical Si nanocrystals enclosed in stoichiometric silicon oxide.

The most common method for investigating the light emitting properties of Si nanocrystals is photoluminescence (PL) whereby photons with energy greater than the band gap excite free carriers across the gap which radiatively recombine. One main disadvantage of this technique is the lack of high spatial resolution, which is limited by the size to which the spot can be focused and the absorption depth of the material. Consequently overlying material of the substrate may also contribute to the PL signal and make interpretation of the spectra difficult. Techniques such as controlled etching[5,7] have been used to overcome this limitation however these are time consuming and the destructive nature means the sample luminescence may be modified.

Cathodoluminescence (CL) on the other hand offers the advantage of relative simplicity and speed in determining the spatial distribution of luminescence centres because of the relatively small interaction volume of the electrons. In this technique outer shell electrons are excited by the electron beam and radiatively recombine. The diffusion length of these carriers is relatively short in SiO_2, which allows high spatial resolution results.

Unfortunately there have been relatively few CL studies on Si nanocrystals. The study of CL from SiO_2 implanted with Si to sufficiently high dose to result in nanocrystal precipitation has not yet been measured to our knowledge. Work has primarily focused on porous Si (p-Si)[8,9], which is composed of a network of Si nanocrystals and wires, however the stability of the luminescence has been a significant problem. In addition, the optical properties of p-Si may arise from fundamentally different mechanisms to those operating in Si nanocrystals dispersed in SiO_2[10], so p-Si cannot necessarily

[1] Current address: S-SENCE and Applied Physics, Linköping University, SE-581 83 Linköping, Sweden

Photonics: Design, Technology, and Packaging II, edited by Derek Abbott, Yuri S. Kivshar, Halina H. Rubinsztein-Dunlop, Shanhui Fan, Proc. of SPIE Vol. 6038, 60380J, (2006) · 0277-786X/06/$15 · doi: 10.1117/12.638662

be regarded as a representative system. CL has been used extensively to study the matrix material amorphous SiO_2, including Si implanted SiO_2[11 and refs therein]. Relatively high beam energies are typically used (> 8 keV) because sample preparation generally results in surface damage causing a dead (nonluminescent) layer. The main luminescent centres emitting in the visible region are two-fold coordinated Si with a blue peak at 2.7 eV and the non-bridging oxygen hole centre with a red peak at 1.85 eV[11].

In this paper we present CL spectra from Si-implanted SiO_2 before and after annealing showing that the appearance of an intense CL band at 800 nm is associated with the formation of Si nanocrystals, which agrees with PL measurements by other groups. In addition, we present results on determining the depth-resolved luminescence in the sample. We use simulations to show that the maximum entropy (MaxEnt) method is the most appropriate technique to solve the underlying inverse problem, and use the experimental CL intensity data to demonstrate that the 800 nm CL coincides with the Si nanocrystal depth.

2. EXPERIMENTS

Fused silica slides were ion implanted at room temperature with 600 keV Si^+ ions to doses of 1.3×10^{17} and 2.6×10^{17} cm^{-2} (referred to as "low" and "high" doses). SRIM code[12] was used to model the ion depth distribution and predicted a peak concentration at ~ 850 nm. The samples were annealed at 1100°C for 60 min under a nitrogen atmosphere to precipitate the nanocrystals, then at 500°C for 60 min under a forming gas atmosphere ($95\%N_2/5\%H_2$) to passivate the material and increase the nanocrystal luminescence intensity[4]. We expect the nanoparticles to have sizes in the range 3-6 nm[6]. Since the nucleation and growth of nanocrystals is strongly dependent on local excess Si concentration, we expect the largest nanocrystals at ~ 850 nm and smaller nanocrystals above and below this depth. Before any CL measurements were performed, the samples were carbon coated and the edges painted with silver paint to prevent charge build-up under the electron beam.

The CL experiments in this study were performed using an Oxford Instruments Mono CL2 system installed on a JEOL35C SEM. The CL signal was detected using a Hamamatsu R943-02 Peltier-cooled photomultiplier tube. Measurements were made at room temperature over the wavelength range 350-900 nm with a resolution of 10 nm, with a collection time of about 3 min 15 s for each spectrum. The electron beam current was measured with a Faraday cup. All spectra were corrected for system response.

By varying the energy of the electron beam the excitation region changes in depth thus permitting depth-resolved CL measurements. The CL spectra were measured using a scanning beam with energy from 4-25 keV and the beam current adjusted within the range 5-30 nA so that the total power was a constant at all measurements, the so called "constant power method"[13]. With this method a constant depth distribution of luminescent centres would give a constant CL intensity as the beam energy is varied. Deviations from this distribution are reflected in the CL intensity. Gaussian fits were made to the peaks in the spectra to identify peak wavelength and integrated intensity. The integrated intensity under a given band as a function of electron beam energy was used for the depth profile analysis.

3. DEPTH PROFILE ANALYSIS

An empirical model of the energy transferred to a SiO_2 sample as a function of depth and beam energy is given by[11]

$$\frac{dE}{dz} = 1.544\frac{E_0}{R}\exp\left[-7.5\left(\frac{z}{R}-0.3\right)^2\right] \tag{1}$$

with the initial beam energy E_0 in keV and the maximum electron range R in nm given by

$$\begin{aligned} R &= 38.5E_0^{1.3}, E_0 < 10keV \\ R &= 22.1E_0^{1.7}, E_0 > 10keV \end{aligned}. \tag{2}$$

The CL intensity is given by the product of the energy deposited in the samples and the number of luminescence centres $n(z)$:

$$I(E_0) = c\int_0^d \frac{dE}{dz}(z, E_0)n(z)dz\,. \tag{3}$$

The problem of determining the depth profile from the recorded CL data is a linear inverse problem. That is, given the CL intensities and knowledge concerning the energy transfer function, we want to determine the depth profile. Moreover, we want to determine the profile without making any assumptions about the profile distribution functions. In other words, in solving the inverse problem, we are seeking to determine a *free form* or *non-parametric* solution[14]. This general approach ensures that depth profile is not restricted by a specific distribution function. It also ensures that the underlying physics can be full investigated without being limited by specific assumptions imposed by the definition of the distribution function.

The first step towards to solving the inverse problem is to recognise that the integral equation defined in (3) can be transformed into a matrix-vector equation

$$\mathbf{g} = \mathbf{A}\mathbf{p} + \mathbf{n} \tag{4a}$$

where **g** is the $[N \times 1]$ vector consisting of CL intensity data; A is a $[N \times M]$ energy transfer kernel matrix, such that $N \geq M$; **n** is the $[N \times 1]$ noise distribution, where $\langle \mathbf{n} \rangle = 0$ and $\sigma_i \propto \sqrt{g_i}$; and p is a $[M \times 1]$ vector depth profile, such that,

$$p_j \geq 0\,, \quad \forall\, j \tag{4b}$$

and

$$\sum_j p_j = 1\,. \tag{4c}$$

The properties of the energy transfer matrix, **A**, dictate the conditioning of the solution profile, **p**. If **A** is near-singular, such that with det $\mathbf{A}^T\mathbf{A} \sim 0$, then the noise in (4a) will be amplified when evaluating the inverse of $\mathbf{A}^T\mathbf{A}$. Consequently, the underlying depth profile will be rendered meaningless due to the presences of spurious oscillations in the solution depth profile, while conditions (4b) and (4c) will not be preserved. This describes the failure of the usual least-squares solution, $(\mathbf{A}^T\mathbf{A})^{-1}\,\mathbf{A}^T\,\mathbf{g}$.

There are number of approaches which can be employed to determine depth profile (4a). Below, we outline two such approaches, namely the regularisation and maximum entropy methods. A full mathematical analysis and discussion of the former can be found in Armstrong and Kalceff[15] (see references therein), while a full discussion and references of the later can be found in Sivia[14] and Armstrong *et al*[16].

The near-singular nature of $\mathbf{A}^T\mathbf{A}$ means that the solution depth profile will be swamped by spurious oscillations as a result of the amplification of the noise in (4a). The regularisation method stabilises the inverse $\mathbf{A}^T\mathbf{A}$ by constraining (4a) with $\mathbf{p}^T\mathbf{p}$. On maximising the resulting Lagrangian equation produces[15]

$$\mathbf{p} = \left(\alpha\mathbf{I} + \mathbf{A}^T\mathbf{A}\right)^{-1}\mathbf{A}^T\mathbf{g} \tag{5}$$

where **I** is a $[M \times M]$ identity matrix, $0<\alpha<\infty$ is the Lagrangian parameter, which is selected to stabilise the inverse matrix $\left(\alpha\mathbf{I} + \mathbf{A}^T\mathbf{A}\right)$. This approach can be extended to include a Bayesian formulation to determine the most probable value for α (see Ref 14). Also an additional Lagrangian parameter could be include to ensure that the positivity constraint is preserved, (4b), but this requires imposing additional assumptions on the Lagrangian function and determining the values for two parameters. That is, the quadratic form of $\mathbf{p}^T\mathbf{p}$ does not preserve the positivity of the solution, but does attempt to stabilise $\mathbf{A}^T\mathbf{A}$ matrix.

The application of the maximum entropy method centres on solving linear inverse problems, (4a) by using an entropy function. This method ensures that (4b) and (4c) are preserved[14]. The rational of the maximum entropy method is that by maximising the entropy function constrained by the experimental data, the solution (i.e. depth profile) with the least assumptions can be determined[14]. This entropy function for **p** is given by,

$$S = -\sum_j p_j \ln(p_j / m_j) \tag{6}$$

where **m** is $[M \times 1]$ is the default model profile distribution, usually taken to be uniform distribution as $1/N$, while the logarithm in (6) ensures that solutions with only positive values are considered. Equation (6) is constrained by a likelihood function that includes the experimental data, uncertainties and profile distribution,

$$\begin{aligned} L &= \sum_i \left(g_i - \sum_j A_{ij} p_j \right)^2 / \sigma_i^2 \\ &= \chi^2 / 2 \end{aligned} \tag{7}$$

where σ are the uncertainties associated with **g**. In order to couple the functions in (6) and (7), a Lagrangian multiplier is $0<\alpha<\infty$ is defined, and the corresponding Lagrangian function,

$$Q = \alpha S - L . \tag{8}$$

It is interesting to point out that the regularisation method is a quadratic approximation of (6), while in order to recover the depth profile from a linear inverse problem, it is necessary to introduce a nonlinear regularisation functions, such as (6). There are many arguments why (6) is preferred over other functions which preserve (4b) and (4c). Ref. 14 provides a useful introduction and outline for the arguments for using (6).

In the present study we use the Skilling & Bryan algorithm[17] to determining α-value and the profile distribution. Due to the nonlinear properties of (6), Skilling & Bryan algorithm solves (8) iteratively. The algorithm steps toward $L_{\text{aim}}=N$, where N is defined by the number of data points, and a α-value and **p** is determined which maximise (6), while ensuring that ∇S is (near-)parallel to ∇L.

4. RESULTS AND DISCUSSION

4.1 CL spectra

Unannealed Si implanted SiO_2 is believed to contain few or no Si nanocrystals. A typical CL spectrum is shown in Fig. 1 (squares). Distinct CL peaks are observed at 470 nm and 670 nm. The emission at these wavelengths is known to be associated with defect centres. The blue peak results from recombination at a Si atom with two unbound electrons, called an "oxygen deficient centre" (ODC) and the red peak is associated with an oxygen atom with one unbound electron, a "non-bridging oxygen hole centre" (NBOHC) (see Ref. 11). These same spectral features are also observed in CL from unimplanted SiO_2 (also shown in Fig. 1), an observation made also by other groups[11]. For our samples the red peak intensity is not affected by implantation but the blue peak increases in intensity reflecting the increase in ODCs as a result of the excess Si in the SiO_2.

The CL spectrum from the annealed material which contains Si nanocrystals is shown in Fig. 2. The blue ODC emission does not change appreciably in intensity with annealing, but an intense infrared peak appears centred at about 850 nm. This peak is very similar to the Si nanocrystal PL band reported by groups studying similar samples[4,6]. Some previous results of CL from p-Si show the ODC and NBOHC bands and an IR band at 750 nm[8,9] although it is not clear in these measurements if the red NBOHC emission is still present because of the broad overlapping IR band. The CL from an annealed unimplanted sample (not shown) did not show any emission in the blue or IR. This confirms that the IR is related to the nanocrystals rather than the matrix, and the removal of the ODC peak indicates that the annealing conditions are sufficient to reconstruct damage to the silica matrix due to polishing.

The peak energy of the IR band depends on dose; by decreasing implant dose the IR band shows a blueshift from 860 nm to 800 nm as shown in Fig. 3. This observation is consistent with attributing this band to nanocrystal emission and agrees with the dose dependence seen in Si nanocrystal PL by Cheylan *et al*[4] and Ross *et al*[6]. The nanocrystal size is expected to decrease with the amount of excess Si in the silica so quantum confinement effects will consequently blueshift the emission.

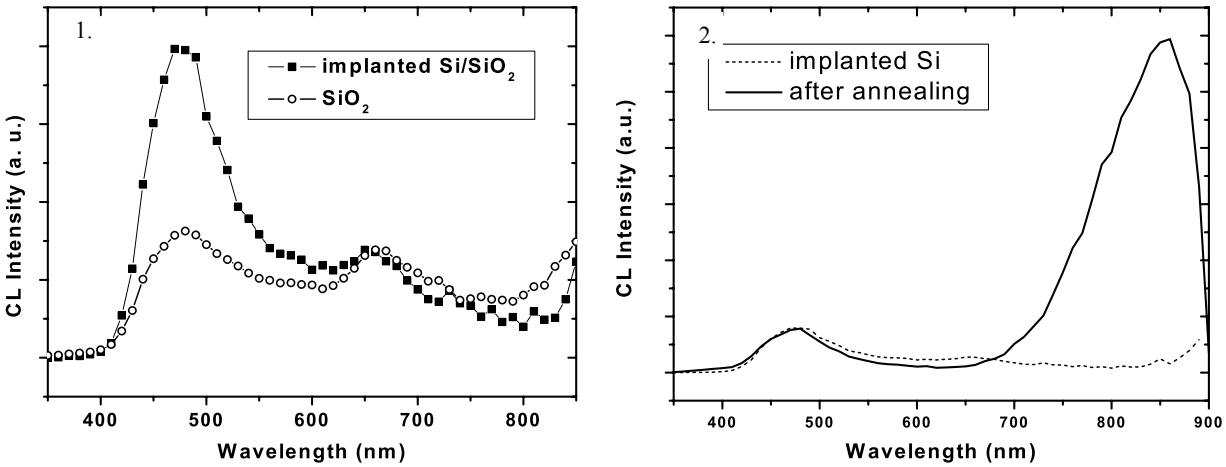

Fig. 1. CL spectra of polished fused silica (circles) and low dose Si implanted silica (squares) at 18 keV and 100 nA.
Fig. 2. CL spectra of high dose as-implanted silica (dotted line) and annealed implanted silica (solid line), at 15 keV and 30 nA.

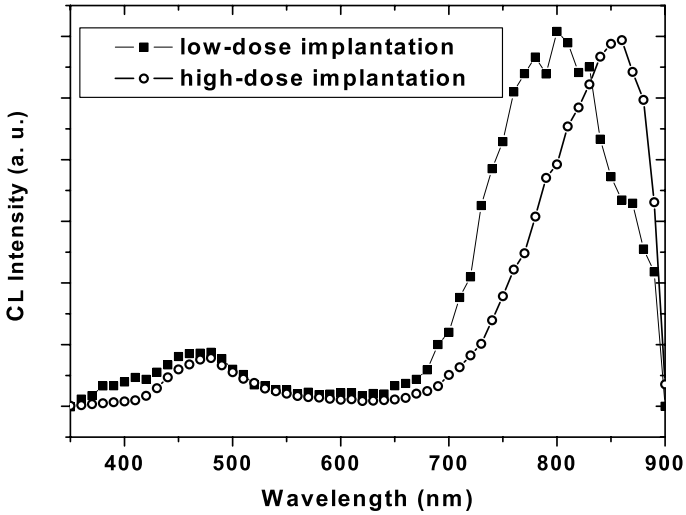

Figure 3. Room temperature CL spectra from annealed SiO_2 implanted with Si: low dose (squares, 20 keV) and high dose (circles, 18 keV).

4.2 CL depth resolution: simulations

In order to demonstrate the application of regularisation and MaxEnt methods described above, CL data were simulated using (4a). The energy transfer matrix was defined as a [26×26] matrix using (1) over energy range of 5 keV to 30 keV and over the depth range of 0 nm to 2000 nm. The depth profile distribution with dimensions [26×1] column vector was defined by a Gaussian distribution with $\langle x \rangle$ = 200 nm and σ_x = 700 nm. This distribution defined the *true depth profile*.

Four simulated CL intensity profiles were generated for different levels of heteroscedastic Gaussian noise. The simulated CL intensities were scaled such that noise level in the maximum amplitude was 0.1%, 0.5%, 1.0% and 5.0% (i.e. 1.0×10^6 counts, 4.0×10^5 counts, 1.0×10^4 counts and 4.0×10^2 counts, respectively). The simulated CL intensities are given in Fig. 4. For each set of simulated CL data, the depth profile was determined using the regularisation method (5), and MaxEnt method (8). The misfitting between the solutions depth profile relative to the true depth profile was defined by

$$R_f = \left[\frac{\sum_j \left(p_{true\,j} - p_{sol\,j} \right)^2}{\sum_j p_{true\,j}^{\,2}} \right] \times 100\% \,. \tag{6}$$

Both the regularisation and MaxEnt methods were applied to simulated data. The energy transfer kernel matrix was evaluated and det $\mathbf{A}^{\mathbf{T}}\mathbf{A}$ was calculated to be $<10^{-50}$, which implies that the kernel is ill-conditioned and many solutions for **p** may exist.

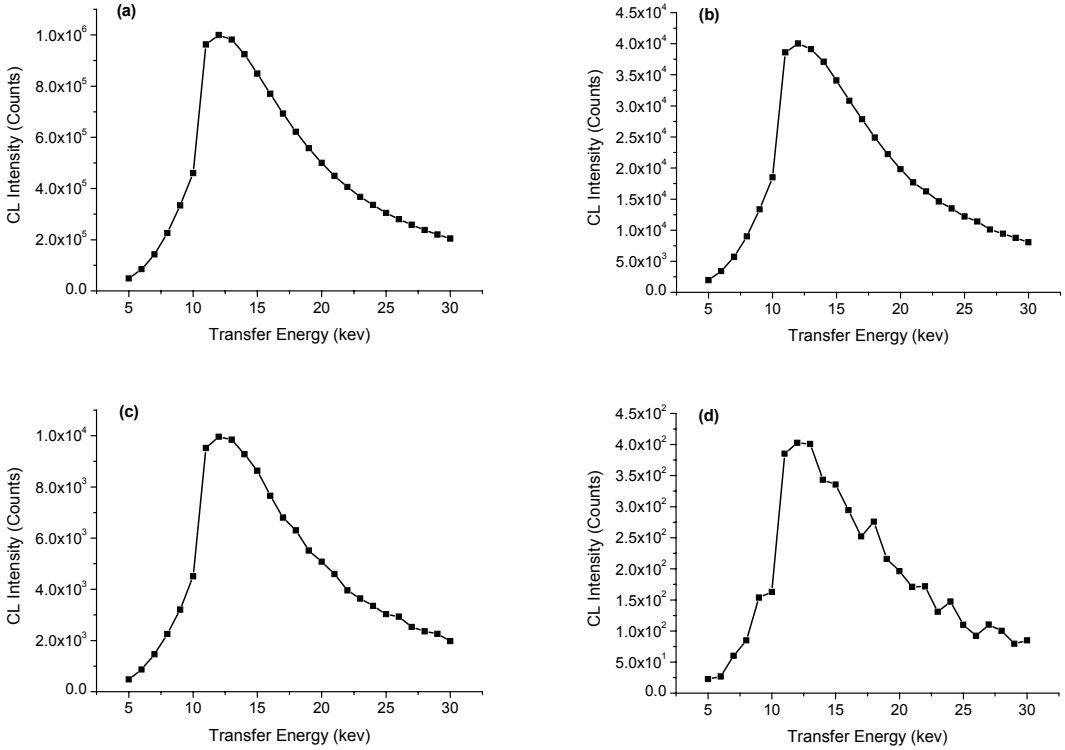

Figure 4. Simulated CL Intensity distributions as a function of the transfer energy for different levels of noise: (a) for 0.1% levels of noise; (b) 0.5% levels of noise; (c) 1.0% levels of noise; (d) 5.0% levels of noise.

The results for regularisation and MaxEnt methods are given in Fig. 5, for the above stated noise levels. The R_f-factors for both methods are also given in Table 1.

Relative Noise Level (%)	Regularisation Method (%)	MaxEnt Method (%)
0.1	15.7 ($\alpha=5.0\times10^{-5}$)	10.2 ($\alpha=7.9\times10^{-6}$)
0.5	15.7 ($\alpha=1.0\times10^{-4}$)	10.7 ($\alpha=2.0\times10^{-4}$)
1.0	19.0 ($\alpha=5.0\times10^{-4}$)	12.0 ($\alpha=6.5\times10^{-4}$)
5.0	30.8 ($\alpha=1.0\times10^{-3}$)	22.4 ($\alpha=4.0\times10^{-3}$)

Table 1: R_f-factors results for Regularisation and MaxEnt methods for four different levels of noise.

For low levels of noise, both methods are able to reproduce the depth profile, without making any assumptions about the profile distribution function. This is demonstrated by the fact that a uniform default model **m**, in (6), was defined over the range of depths. Using this as the starting point, the MaxEnt method resolves the depth profile (see Fig. 5). Although this is not explicitly defined in (5), it is an underlying assumption of the method.

The regularisation and MaxEnt solutions can be compared to the true depth profile. In Fig. 5(a) some fluctuations are noticeable due to the presence noise in the data for both methods, but this is small. However, it is noticeable that the regularisation method produces negative values about the baseline, while it is more sensitive to the noise in the data, as indicated by Table 1. As the noise level increases from 0.1% to 1.0%, the R_f-factor in both methods increases marginally. The influence of the noise can be seen for the results in Fig. 5 (a-c). At 5% noise level the R_f-factor values have increase considerably for both methods (see Table 1 and Fig. 5(d)). The misfitting between the solution and true distributions in both methods can be seen in the loss of amplitude, additional broadening in the solution distributions and shift of peak maximum (see Fig. 5(d)). The presences of these artefacts can influence the interpretation of the CL data and may result in erroneous conclusions being drawn from the data and analysis. However, for 5% noise level, improvements in the solution profile can be produced by defining a non-uniform default model to be applied in the MaxEnt method[16]. Moreover, using a Bayesian approach the plausibility of the non-uniform model can be assessed[14].

The exercise in simulating the CL data and recovering the depth profile using the regularisation and MaxEnt methods demonstrate that a free form solution can be determined from (3). In addition, the MaxEnt method preserves conditions (4b) and 4(c) over a large range of noise levels.

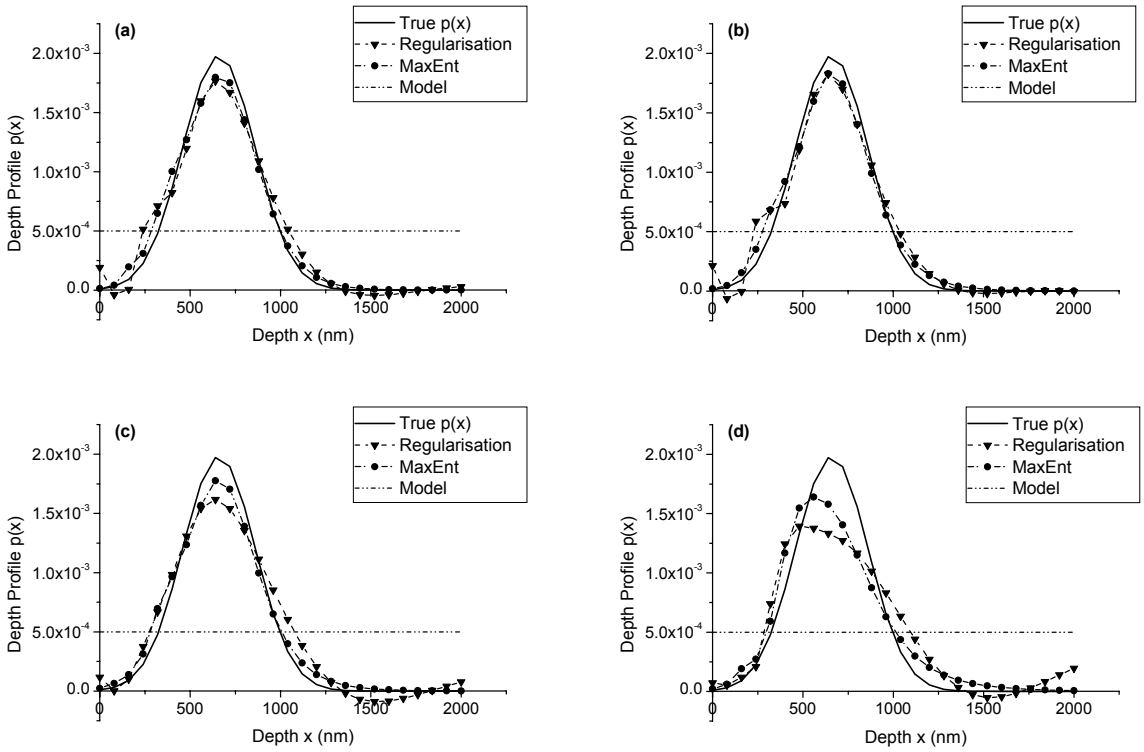

Figure 5: Solution depth profiles using the Regularisation method, MaxEnt method and MaxEnt model compared to the true depth profile for different levels of noise: (a) Solutions depth profiles for 0.1% noise in CL data; (b) Solutions depth profiles for 0.5% noise in CL data; (c) Solutions depth profiles for 1.0% noise in CL data; (d) Solutions depth profiles for 5.0% noise in CL data.

4.3 CL depth resolution: experimental results

In order to determine the depth profile of the IR and blue luminescent centres in the material, CL spectra were measured using the constant power method with a range of different beam energies. A plot of integrated IR peak intensity as a function of electron beam energy for the high dose sample is shown in Fig. 6. The data do not fall on a straight

horizontal line, which would indicate a constant depth profile; rather they rise from zero, peak at 11 keV and gradually decrease again. This suggests the luminescent centres lie in a narrow band below the surface. There was no peak shift or change in width observed within uncertainty as the accelerating voltage was changed, so we conclude that the CL is dominated by nanocrystals of a size that luminesce at $\lambda \sim 850$ nm.

The depth profiles of the IR luminescent centres generated by the regularisation and MaxEnt methods are shown in Fig.s 7(a) and 7(b). Both profiles show the highest concentration of nanocrystals contributing to the 850 nm band is at a depth of 400 nm and the concentration gradually decrease to zero with depth, however the regularisation solution starts to increase again from 1000 nm while the MaxEnt solution continues to decrease. The regularisation solution also has negative values below 100 nm which are clearly unphysical. For comparison, the excess Si concentration modelled using SRIM is also shown in Fig. 7 from which we can predict that the largest nanocrystals are located near the centre of the implanted region and smaller nanocrystals are located nearer the surface as well as the deeper part of the implanted region[5,6] in line with the supersaturation dependence of particle size in classical particle coarsening theory[18].

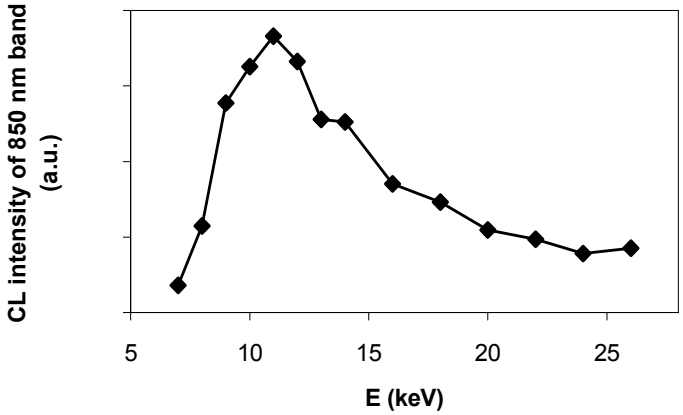

Figure 6. Integrated intensity of the IR band centred at 850 nm from the high dose sample taken as a function of electron beam energy. The product of beam energy and current was 100 kV.nA.

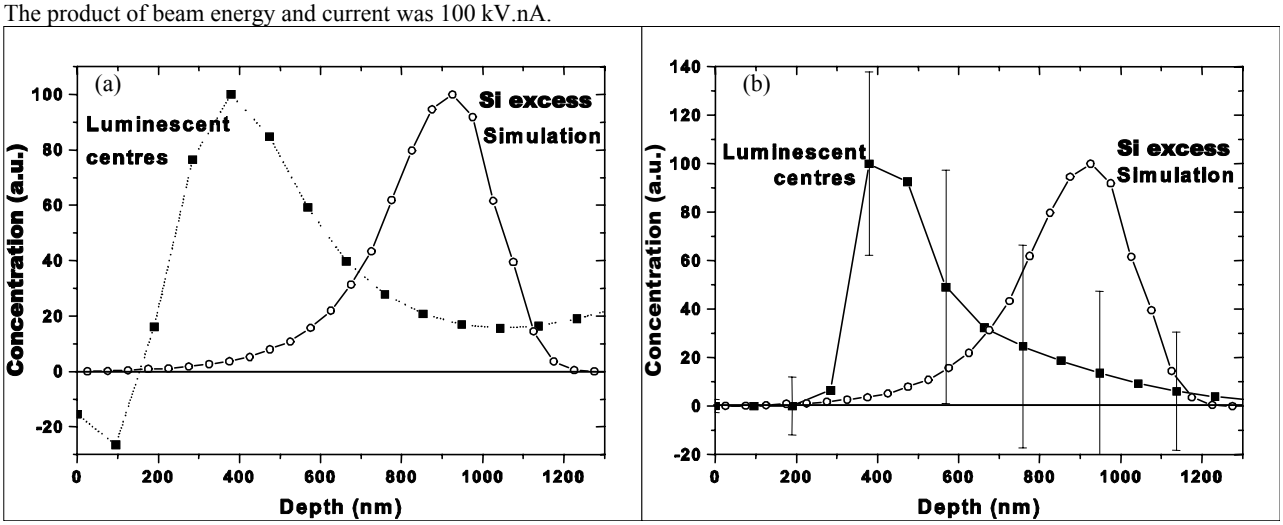

Figure 7.(a) Regularisation solution and (b) MaxEnt solution of depth profile of concentration IR emitting centres in high dose sample obtained from the data in Fig. 6. A plot of the depth dependence of excess Si simulated with SRIM is also shown, normalised to the solution peak height.

In general, the CL efficiency and wavelength depend on the nanocrystal size distribution, which will affect the luminescent nanocrystal profile. As shown in Fig. 7, the most intense 800 nm CL is not the centre of the implanted region, but towards the surface, where the excess Si concentration drops below 3 at.% and the nanocrystals are very small. Similar results were seen by Brongersma *et al*[5] who used controlled etching and PL to study depth resolved

luminescence of Si nanocrystals in Si implanted SiO_2. They showed that 900 nm PL (from largest nanocrystals) was most intense in the middle of the implanted region and 700 nm PL (from smallest nanocrystals) originated from regions on either side of the implanted band. We therefore conclude this IR band is predominantly due to CL from relatively small nanocrystals in the near surface region. Improved CL spectral resolution would allow inspection of the 700 nm and 900 nm contributions to confirm this interpretation.

During a measurement on a single spot, it was noticed that the peaks changed in intensity until reaching a steady intensity level. The blue ODC peak increases slightly while the IR nanocrystal peak reduced in intensity by 50%. The exact radiolysis mechanisms behind these changes are not yet identified. However, modification of peak intensity with electron dose plays an important role in the accuracy of the intensity values used for depth profiling. We attempted to characterise the decay of the IR peak and the growth of the blue peak as a function of electron energy and these corrections are included in the data analysis here, and further refinements to this characterisation will be reported in future publications.

5. CONCLUSIONS

In conclusion, we have demonstrated that CL is a powerful technique capable of resolving the IR luminescence of Si nanocrystals in a SiO_2 matrix. We have shown that Si implantation causes an increase in blue CL due to the increase in the number of ODCs, and that the formation of nanocrystals results in a large IR peak, in agreement with PL measurements by other groups. By simulating noisy CL data we have shown that the depth profile of luminescent centres can be recovered using the MaxEnt technique, which preserves the positivity and additivity of the solution. We have applied this technique to experimental data of IR luminescence from Si nanocrystals and have shown that contributions to this band are dominated by smaller nanoparticles halfway between the surface and depth at which peak excess Si is located.

ACKNOWLEDGEMENTS

The authors would like to thank R.G. Elliman of the Australian National University for the nanocrystal samples used in this study. We also acknowledge the technical assistance of N. Booth, K. McBean and A. Vella. This work was supported by the UTS ECR Research Grant Scheme.

REFERENCES

1. Z.H. Lu, D.J. Lockwood, and J.-M. Baribeau, "Quantum confinement and light-emission in SiO_2/Si superlattices", *Nature*, **378**, pp. 258-260, 1995.
2. L.H. Abuhassan, M.R. Khanlary, P. Townsend, and M.H. Nayfeh, "Cathodoluminescence of small silicon nanoparticles under electron beam excitation", *J. Appl. Phys.*, **97**, pp. 104314-1-5, 2005.
3. A.K. Kalkan, S.J. Fonash, and S.C. Cheng, "Band-tail photoluminescence in nanocrystalline Si", *Appl. Phys. Lett.*, **77**, pp.55-57, 2000.
4. S. Cheylan, N.B. Manson, R.G. Elliman, "Dose dependence of room temperature photoluminescence from Si implanted SiO_2", *J. Lumin.*, **80**, pp.213-216, 1998.
5. M.L. Brongersma, A. Polman, K.S. Min, and H.A. Atwater, "Depth distribution of luminescent Si nanocrystals in Si implanted SiO_2 films on Si", *J. Appl. Phys.*, **86**, pp.759-763, 1999.
6. G.G. Ross, R. Smirani, V. Levitcharsky, Y.Q. Wang, G. Veilleux, and R.G. Saint-Jacques, "Effect of Si implantation on the microstructure of silicon nanocrystals and surrounding SiO_2 layer", *Nucl. Instrum. Methods B*, **230**, pp.198-202, 2005.
7. U. Serincan, G. Aygun, R. Turan, "Spatial distribution of light-emitting centres in Si-implanted SiO_2", *J. Lumin.*, **113**, pp. 229-234, 2005.
8. M. Itoh, N. Yamamoto, and O. Nittono, "Cathodoluminescence imaging of n-type porous silicon", *Jpn. J. Appl. Phys. Pt 1*, **35**, pp. 4182-4186, 1996.
9. A.G. Cullis, L.T. Canham, G.M. Williams, P.W. Smith, and O.D. Dosser, "Correlation of the structural and optical-properties of luminescent, highly oxidised porous silicon", *J. Appl. Phys.*, **75**, pp. 493-501, 1994.
10. N. Daldosso, M. Luppi, S. Ossicini, *et al*., "Role of the interface region on the optoelectronic properties of silicon nanocrystals embedded in SiO_2", *Phys. Rev. B*, **68**, pp.085327-1-8, 2003.
11. H.-J. Fitting, T. Barfels, A.N. Trukhin, B. Schmidt, A. Gulans, and A. von Czarnowski, "Cathodoluminescence of Ge^+, Si^+, and O^+ implanted SiO_2 layers and the role of mobile oxygen in defect transformations", *J. Non-cryst. Sol.*, **303**, pp.218-231, 2002.

12. J.F. Ziegler, J.P. Biersack, and U. Littmark, *The Stopping and Range of Ions in Solids*, Pergamon Press, New York, 2003.
13. A.P. Young, R. Bandhu, J. Schafer, H. Niimi, and G. Luckovsky, "Cathodoluminescence spectroscopy of nitrided SiO_2-Si interfaces", *J. Vac. Sci. Technol. A*, **17**, pp. 1258-1262, 1999.
14. D.S. Sivia, *Data Analysis: A Bayesian Tutorial*, Clarendon Press, Oxford, 1996.
15. N. Armstrong and W. Kalceff, "Eigen-system analysis of X-ray diffraction profile deconvolution methods explains ill-conditioning" *J. Appl. Cryst.*, **32**, pp. 453-460, 1998.
16. N. Armstrong, W. Kalceff, J.P. Cline, and J. Bonevich, "Bayesian inference of nanoparticle broadened X-ray line profiles", *J. Res. Natl. Inst. Techn.*, **109**, pp. 155-178, 2004.
17. J. Skilling and R.K. Bryan, "Maximum entropy image reconstruction: general algorithm", *Mon. Not. R. Astron. Soc.*, **211**, pp. 111-124, 1984.
18. L.A. Nesbit, "Annealing characteristics of Si-rich SiO_2-films", *Appl. Phys. Lett.*, **46**, pp.38-40, 1985.